Original Research Article

Exploring Reversible Hydrogen Storage Efficiency of R-Substituted [M-doped Imidazoline-Li)]$^+$ Complexes [R= -CF_3, -CN, -CH_3 and M= C, Si, Ge]; An *In-silico* Study

Abhishek Bag [1,2], Anupam Aash [1,3], Dilip K. Debnath [3,*], G. Naaresh Reddy [4,*], Gourisankar Roymahapatra [1,*]

[1] *Department of Applied Sciences, Haldia Institute of Technology, Haldia 721657, WB, India*
[2] *Department of Basic Science & Humanities, Global Institute of science and Technology, Haldia 721657, WB, India*
[3] *Department of Chemistry, Cooch Behar Panchanan Barma University, Cooch Behar 736101, WB, India*
[4] *Department of Chemistry, Vardhaman College of Engineering, Hyderabad 501218, India*

Citation **A. Bag, A. Aash, D.K. Debnath G.N. Reddy, G. Roymahapatra**. Exploring Reversible Hydrogen Storage Efficiency of R-Substituted [M-doped Imidazoline-Li)]$^+$ Complexes [R= -CF_3, -CN, -CH_3 and M= C, Si, Ge]; An *In-silico* Study. *J. Eng. Ind. Res.* **2025**, 6 (3):244-260.

https://doi.org/10.48309/jeires.2025.514956.1185

Article info:
Submitted: 2025-04-04
Revised: 2025-05-09
Accepted: 2025-05-27
ID: JEIRES-2504-1185

Keywords:
Hydrogen storage, DFT, Bonding interactions, Gravimetric Wt%.

ABSTRACT

This article presents a comprehensive computational investigation on the hydrogen storage efficacy of R-substituted [M-doped Imidazolene-Li)]$^+$ complexes; [R represents –CF_3, –CN, or –CH_3, and M denotes C, Si, or Ge] in the light of density functional theory (DFT). Optimized structures of both the initial complexes and their hydrogen-loaded analogues reveal that the nature of the substituent and the identity of the central atom (C, Si, and Ge) significantly affect the electronic properties and aromaticity of the systems. Global reactivity parameters and aromaticity values indicate that –CN substitutions enhance electron-accepting tendencies, particularly in the C-based complexes, while Si and Ge-based systems display increased electronic softness. Progressive adsorption of H_2 molecules results in decreasing average adsorption energies, underscoring the favorable stabilization upon hydrogen uptake. NBO charge analyses reveal a decrease in the positive charge at the Li center with successive H_2 adsorption, and both ELF and NCI plots confirm that the interactions with hydrogen are predominantly non-covalent. Temperature-dependent Gibbs free energy calculations suggest that lower temperatures favor hydrogen adsorption, though selected complexes retain spontaneity at ambient temperature. Gravimetric analyses further demonstrate that C-based complexes achieve higher hydrogen storage capacities, with values reaching up to 13.53 wt%. Additionally, atom-centered density matrix propagation (ADMP) simulations highlight the kinetic stability of these systems at low temperatures, with noticeable desorption at elevated temperatures. Overall, this study emphasizes the critical role of molecular engineering in optimizing hydrogen storage materials for renewable energy applications.

*Corresponding Author: G. Naaresh Reddy, Dilip K. Debnath, Gourisankar Roymahapatra (naareshreddy_vce169@vardhaman.org; ddnath2000@yahoo.com ; grm.chem@gmail.com)

Introduction

Hydrogen storage materials have emerged as a cornerstone in the pursuit of sustainable and renewable energy solutions. As the global energy landscape shifts toward cleaner alternatives, the development of efficient hydrogen storage systems becomes crucial for overcoming the limitations of intermittent renewable sources such as solar and wind power. In today's energy paradigm, hydrogen is celebrated for its high energy density and zero-emission profile, which make it an attractive fuel for a wide range of applications—from portable electronic devices to large-scale power systems and transportation [1-4]. Recent advances in material science have spurred innovative approaches to hydrogen storage, focusing on the design of nanostructured materials and molecular complexes that can adsorb and release hydrogen under ambient conditions. For instance, the study of R-substituted $[R_2\text{-Im(M-Li)}]^+@nH_2$ complexes, where variations in substituents and central metal atoms are fine-tuned, underscores the importance of molecular engineering in enhancing storage capacities and adsorption energies. Such investigations not only reveal the critical role of non-covalent interactions in hydrogen binding but also highlight the influence of electronic properties on the overall storage performance. Looking forward, the future of hydrogen storage materials lies in their integration into the renewable energy infrastructure. Innovations in molecular design and advanced computational simulations are paving the way for materials that can safely store high amounts of hydrogen at ambient temperatures, addressing one of the major challenges in the hydrogen economy. This progress is instrumental in realizing the vision of a hydrogen-powered society, where efficient storage and delivery systems facilitate the seamless transition from fossil fuels to clean, renewable energy [5-9]. The last five years of studies on metal decorated organic frameworks reveal a rich variety of Li-ion–decorated frameworks capable of storing hydrogen with impressive uptake and weight percentages. Aromatic heterocycles (e.g., imidazole and pyrazole) and triazine isomers trap up to 10–11 H_2 molecules, delivering 10–20 wt % at or below 200 K, while alkali-metallated diazines and C_8N_8 cages achieve 8-13 wt % under similar cryogenic conditions. Simple salts like LiF and LiCl excel at very low temperatures (< 55 K), storing 10 H_2 for up to 43 wt % in LiF and 32 wt % in LiCl, and even $Li_{12}C_{60}$ and Li-MOFs show moderate capacities (9 and 2 wt %) at higher temperatures. Together, these results highlight how carefully chosen Li-decoration strategies can tune both gravimetric density and operating temperature for efficient hydrogen storage [10-21]. Our research group also studied different five or six membered aromatic hetero cyclic rings decorated with coin metal [Cu,Ag and Au], where we have studied different N-Cu/N-Ag/N-Au bonds and their different DFT properties. There we have observed that, Cu decorated systems are the best one [22-25]. Overall, the continuous exploration of novel hydrogen storage materials is essential for advancing renewable energy technologies and achieving a sustainable energy future. The research presented in the attached study exemplifies the potential of strategically engineered molecular systems to revolutionize hydrogen storage, making them an indispensable component of the renewable energy sector [26-30].

Experimental

Using Koopmans' theorem, we derived key reactivity parameters—electronegativity, hardness and electrophilicity—from the HOMO and LUMO energies via finite-difference approximations. All R_2 substituted imidazolium–lithium complexes (R = $-CF_3$, –CN, $-CH_3$; M = C, Si, and Ge) and their successive H_2-adducts were fully optimized at the CAM-B3LYP/6-311+G(d,p) level in Gaussian 16, confirming true minima by zero imaginary frequencies. Conceptual DFT descriptors then gauged their chemical stability and reactivity, while average binding and adsorption energies per H_2 molecule quantified interaction strengths. Gravimetric wt % analyses estimated hydrogen storage capacity and Gibbs free-energy changes across temperatures assessed adsorption spontaneity. Aromaticity was

probed through NICS(0) and NICS(1) values, and Multiwfn-based topological studies—including shaded surface maps, electron localization functions and non-covalent interaction analyses—elucidated bonding patterns, collectively guiding the design of robust high-capacity hydrogen storage materials. Details of methodology are in SI file [31-55].

Results and Discussion

Initially, we substituted different systems with various R groups (-CF_3, -CN, -CH_3) and metal centers (M = C, Si, Ge). Subsequently, molecular H_2 was adsorbed onto these systems around the Li center. First, we optimized the R-substituted systems, followed by the optimization of H_2-trapped metal-decorated systems. After optimization, we obtained their energy-minimized optimal structures, as illustrated in Figure 1. Maximum H_2 trapped final optimized structures are presented in Figure 2. The data from Table 1 and Table 2 reveal that the stability of these complexes correlates strongly with both the nature of the central M atom and the substituents attached to the imidazole ligand. For the M = C systems, the shortest M–Li bond distances (approximately 2.02–2.08 Å) and relatively open N–M–N bond angles (around 102–104°) indicate a compact and rigid coordination environment, which is generally associated with higher hardness and greater structural robustness. In contrast, when M is replaced by larger atoms such as Si and Ge, the M–Li bond distances become noticeably longer (ranging from about 2.51 to 2.65 Å for the bare species, and further elongating in the H_2-coordinated systems), while the N–M–N angles decrease—especially in the Ge systems where they approach 84-87°. These longer bonds and reduced angles suggest a less tightly bound and more flexible interaction, pointing to a softer, less robust framework. Moreover, when comparing substituents, the methyl (–CH_3) derivatives consistently exhibit slightly shorter bond distances and marginally wider bond angles compared to the –CF_3 and –CN analogues, indicating that electron-donating groups can enhance rigidity further. Overall, the trend implies that carbon-based complexes are the hardest, while the silicon and germanium analogues, due to their extended bond distances and more acute angles, present a softer binding environment, which may translate to reduced stability under stress or deformation. We then calculated various global reactivity parameters, such as hardness and electrophilicity, which are summarized in Table 1.

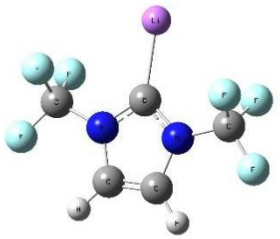
$[(CF_3)_2\text{-Im(C-Li)}]^+$

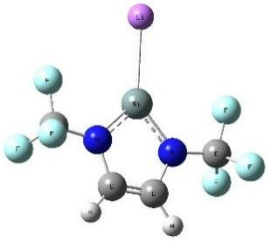
$[(CF_3)_2\text{-Im(Si-Li)}]^+$

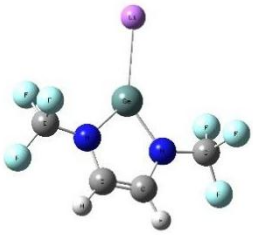
$[(CF_3)_2\text{-Im(Ge-Li)}]^+$

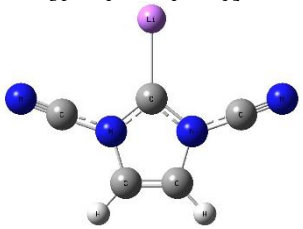
$[(CN)_2\text{-Im(C-Li)}]^+$

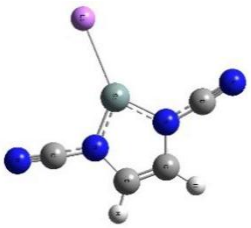
$[(CN)_2\text{-Im(Si-Li)}]^+$

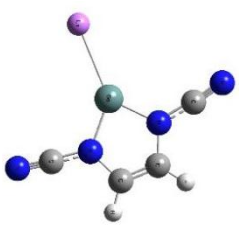
$[(CN)_2\text{-Im(Ge-Li)}]^+$

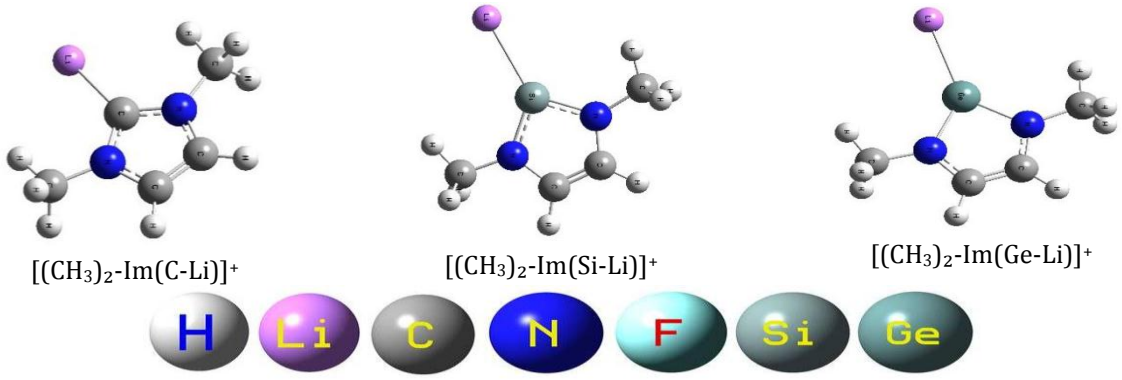

Figure 1: Optimized structure of different $[R_2\text{-Im(M-Li)}]^+$ systems with various R groups (-CF_3, -CN, -CH_3) and metal centers (M = C, Si, Ge) at CAM-B3LYP/6–311+g (d, p) level of theory

Table 1: (a) Electrophilicity (ω, eV); (b) Hardness (η, eV); (c) and (d) are the NICS(0) and NICS(1); (ppm) of R substituted different $[R_2\text{-Im(M-Li)}]^+$ systems [where R= -CF3,-CN ,-CH3 and M= C, Si, and Ge] at CAM-B3LYP/6–311+g (d, p) level of theory

System	Electrophilicity (ω, eV)	Hardness (η, eV)	NICS(0) [ppm]	NICS(1) [ppm]
$[(CF_3)_2\text{-Im(C-Li)}]^+$	4.230	7.849	-13.419	-9.703
$[(CN)_2\text{-Im(C-Li)}]^+$	5.373	8.701	-13.968	-9.491
$[(Me)_2\text{-Im(C-Li)}]^+$	4.231	7.849	-12.479	-11.917
$[(CF3)_2\text{-Im(SiLi)}]^+$	4.634	6.154	-10.026	-6.176
$[(CN)_2\text{-Im(Si-Li)}]^+$	6.550	6.461	-10.717	-6.318
$[(Me)_2\text{-Im(Si-Li)}]^+$	4.634	6.154	-10.052	-7.007
$[(CF3)_2\text{Im(GeLi)}]^+$	4.814	5.757	-10.392	-6.634
$[(CN)_2\text{-Im(GeLi)}]^+$	6.999	5.942	-10.923	-6.676
$[(Me)_2\text{-Im(GeLi)}]^+$	4.814	5.757	-10.702	-7.746

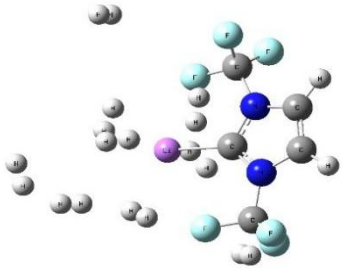
$[(CF_3)_2\text{-Im(C-Li)}]+@9H_2$

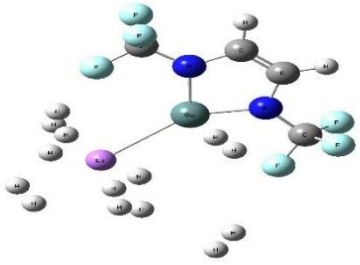
$[(CF_3)_2\text{-Im(Ge-Li)}]+@7H_2$

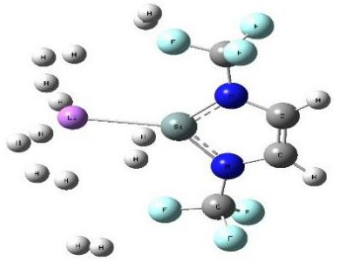
$[(CF_3)_2\text{-Im(Si-Li)}]+@7H_2$

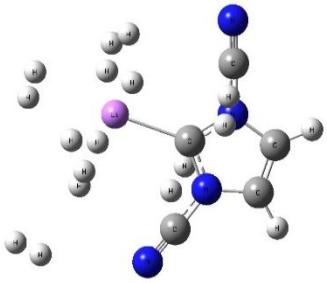
$[(CN)_2\text{-Im(C-Li)}]+@8H_2$

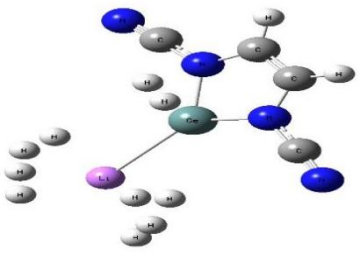
$[(CN)_2\text{-Im(Ge-Li)}]+@5H_2$

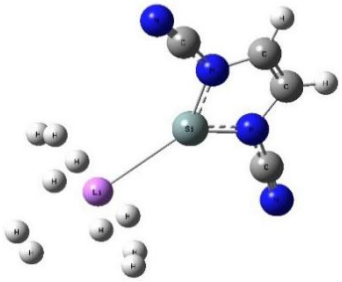
$[(CN)_2\text{-Im(Si-Li)}]+@5H_2$

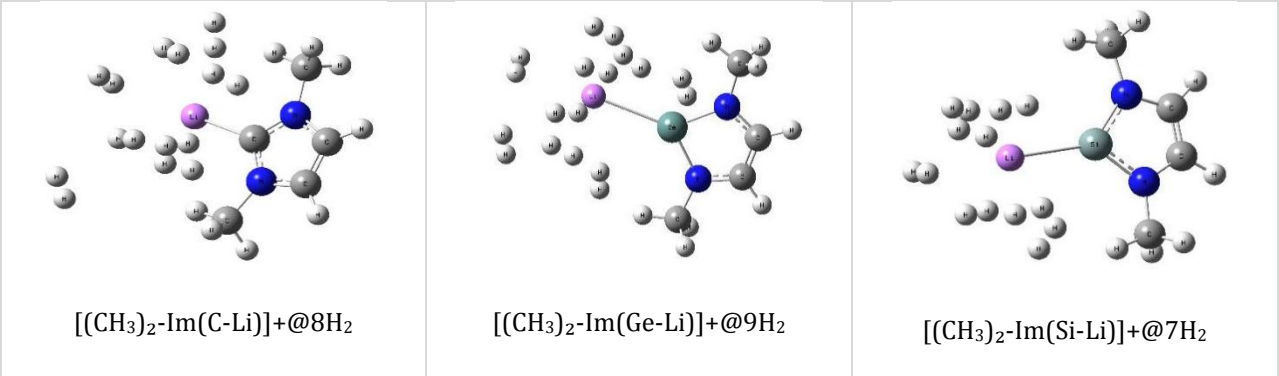

Figure 2: Optimized structure of maximum H_2 trapped different $[R_2\text{-Im(M-Li)}]+@nH_2$ systems with various R groups (-CF_3, -CN, and -CH_3) and metal centers (M = C, Si, and Ge) at CAM-B3LYP/6–311+g (d, p) level of theory

Table 1 indicates that both the substituent type and the central metal atom significantly affect the electronic and aromatic properties of the $[R_2\text{-Im(M-Li)}]+$ systems. For the C-Li series, the –CN substitution leads to higher electrophilicity (5.37 eV) and hardness (8.70 eV) compared to the $–CF_3$ and $–CH_3$ analogues, with the latter showing slightly less negative NICS(0) values and, in the case of $–CH_3$, a markedly more negative NICS(1) value (-11.92 ppm), suggesting differences in aromatic character. Moving to the Si-Li and Ge-Li systems, all complexes exhibit lower hardness (around 5.76-6.46 eV), indicating increased electronic softness, while the –CN derivatives consistently show higher electrophilicity (6.55 eV for Si-Li and 7.00 eV for Ge-Li), which points to a stronger electron-accepting tendency. Additionally, the NICS values become less negative in the Si-Li and Ge-Li series compared to the C-Li counterparts, reflecting a reduction in aromatic stabilization. These variations underscore how the interplay between substituents ($–CF_3$, –CN, $–CH_3$) and the choice of central atom (C, Si, and Ge) modulates the reactivity and stability of these complexes.

Table 2 indicates different parameters reveal distinct electronic and magnetic characteristics that depend on both the substituents and the central atom. In the C-Li systems, for instance, the $[(CN)_3\text{-Im(C-Li)}]^+$ isomer exhibits a higher electrophilicity (4.84 eV) compared to its $[(CF_3)_2\text{-Im(C-Li)}]^+$ (3.86 eV) and $[(CH_3)_2\text{-Im(C-Li)}]^+$ (3.03 eV) counterparts, indicating a greater propensity to accept electrons, while also showing a moderate hardness (~8.9 eV) that suggests a balance between reactivity and stability. Moving to the Si-Li systems, both electrophilicity and hardness values decrease overall, with electrophilicity ranging from about 3.93 to 5.84 eV and hardness around 6.5–7.0 eV; here, the $[(CN)_2\text{-Im(Si-Li)}]^+$ stands out with the highest electrophilicity, hinting at a more pronounced electron-accepting character. In the Ge-Li series, the isomers generally display even higher electrophilicity (up to 6.31 eV) with relatively lower hardness (approximately 6.1-6.5 eV), which may impart a softer, more adaptable electronic framework during hydrogen adsorption. Additionally, the NICS values reveal notable differences in aromaticity: the C-Li based isomers exhibit more negative NICS(0) and NICS(1) values (around -13 to -9 ppm), suggesting stronger aromatic character, while the Si-Li and Ge-Li analogues show less negative values (approximately -10 to -6 ppm). Overall, these variations underscore how the nature of the R substituents and the choice of M atom (C, Si, or Ge) critically influence the electrophilic, hardness, and aromatic properties of the isomers, thereby affecting their reactivity and stability in H_2 trapping processes.

Table 2: Electrophilicity (ω); (eV),Hardness (η); (eV), NICS(0) and NICS(1); (ppm) values of highest no. of H_2trapped different R substituted $[R_2\text{-Im(M-Li)}]^+$ @nH_2 systems [where R= -CF3,-CN ,-CH3, and M= C, Si, Ge] at CAM-B3LYP/6–311+g (d, p) level of theory

System	Electrophilicity (ω, eV)	Hardness (η, eV)	NICS(0) [ppm]	NICS(1) [ppm]
$[(CF3)_2\text{-Im(C-Li)}]+@9H_2$	3.862	9.503	-13.191	-9.419
$[(CN)_2\text{-Im(C-Li)}]+@8H_2$	4.841	8.887	-13.844	-9.557
$[(CH_3)_2\text{-Im(C-Li)}]+@8H_2$	3.027	8.960	-12.563	-9.281
$[(CF3)_2\text{-Im(Si-Li)}]+@7H_2$	5.066	6.963	-9.766	-6.230
$[(CN)_2\text{-Im(Si-Li)}]+@5H_2$	5.835	6.616	-10.440	-6.233
$[(CH_3)_2\text{-Im(Si-Li)}]+@7H_2$	3.930	6.487	-9.851	-6.923
$[(CF3)_2\text{-Im(Ge-Li)}]+@7H_2$	5.203	6.490	-9.865	-6.339
$[(CN)_2\text{-Im(Ge-Li)}]+@5H_2$	6.309	6.102	-10.669	-6.522
$[(CH_3)_2\text{-Im(Ge-Li)}]+@9H_2$	4.042	6.059	-10.440	-7.987

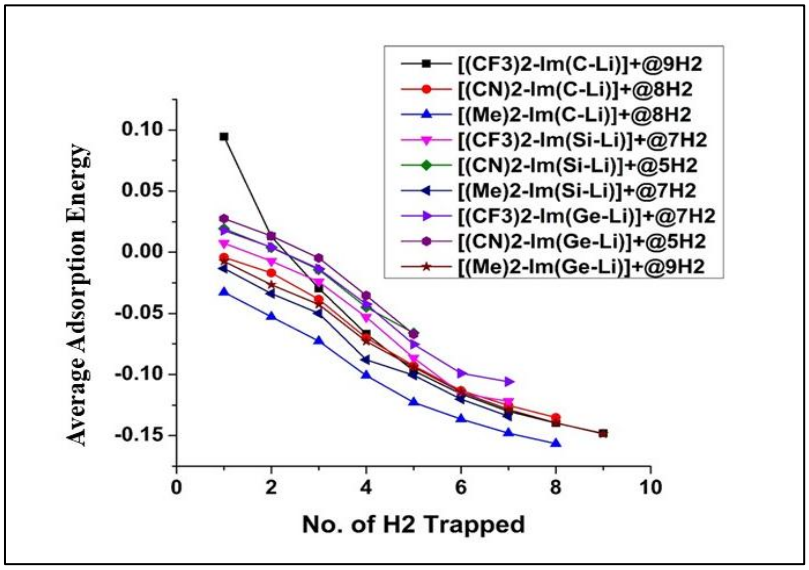

Figure 3: Variation of E_{ads} (eV) (average adsorption energy) with the gradual trapping of H_2 molecules for different R substituted $[R_2\text{-Im(M-Li)}]^+$@nH_2 systems [where, R= -CF_3,-CN ,-CH_3, and M= C, Si, and Ge] at CAM-B3LYP/6–311+g (d, p) level of theory

Figure 3 indicates the variation of average adsorption energy becomes progressively decreased with the gradual trapping of H_2 molecules, indicating that the stabilization of the system increases as more H_2 is adsorbed. Decreasing trends indicates the gradual trapping of H_2 molecule and stability of the model systems. For example, in the $[(CF_3)_2\text{-Im(C-Li)}]^+$ system, the energy starts slightly positive (0.095) with one H_2 molecule and declines to –0.148 by the time nine H_2 molecules are adsorbed, suggesting that initial interactions are weak or even slightly repulsive before turning favorable. In contrast, the –CN and –CH_3 substituted systems, such as $[(CN)_2\text{-Im(C-Li)}]^+$and $[(CH_3)_2\text{-Im(C-Li)}]^+$, exhibit negative adsorption energies from the outset, which continue to drop with increasing H_2 loading (e.g., reaching –0.135 and –0.157, respectively). A similar trend is observed for the Si-Li and Ge-Li analogues, although the maximum number of H_2 molecules varies. Overall, these results demonstrate that both the nature of the substituent (–CF_3, –CN, –CH_3) and the central atom (C, Si, and Ge) play significant roles in modulating the adsorption energy profile, with all systems showing enhanced stabilization at higher hydrogen coverage [56,57]. Table 3 indicates the average adsorption energy values of different systems for the gradual trapping of H_2 molecules. Decreasing trends of NBO charge on Li-metal center indicates the trapping of H_2 molecules on model systems.

Due to this reason, we have performed NBO charge analysis on Li- metal center. The NBO charge analysis (Figure 4) on the Li metal center in various R-substituted [R_2-Im(M-Li)]$^+$@nH_2 systems (with R = -CF_3, -CN, -CH_3, and M = C, Si, and Ge) reveals notable trends in charge distribution upon H_2 adsorption.

For the parent complexes without any H_2 (0 H_2), the Li centers carry relatively high positive charges—ranging roughly from 0.891 to 0.954—with the [$(CN)_2$-Im(C-Li)]$^+$system showing the highest value. As successive H_2 molecules are introduced, a gradual decrease in the NBO charge is observed, suggesting an increasing electron density at the Li center, likely due to electron donation or redistribution from the coordinated H_2 molecules. Although this trend is consistent across all metal centers, subtle variations in the extent of charge reduction reflect the impact of both the substituent type and the nature of the metal (C, Si, or Ge) on the overall electronic environment. This analysis underscores the complex interplay between molecular substitution, metal identity, and gradual hydrogen adsorption on Li center [58,59]. Figure 4 indicates the NBO charges on the Li center of different systems for the gradual trapping of molecular H_2.

Next, we analyze the bonding nature of the H_2-trapped, R-substituted [R_2-Im(M-Li)]+@nH_2 systems (with R = -CF_3, -CN, -CH_3 and M = C, Si, and Ge) at the CAM-B3LYP/6–311+g(d, p) level of theory. To achieve this, we investigated the Electron Localization Function (ELF) plot of the model system to clarify its bonding characteristics. Electron localization function (ELF) determines the extent of the localization of electrons in space and gives a way for electron pair mapping probability in multi-electron systems [22].

As demonstrated in Figure 5, the ELF plot confirms that there is almost no electron density between the metal and the ring or between the metal and the molecular H_2, indicating a non-covalent interaction between the Li metal center and H_2. This non-covalent interaction is further supported by the NCI plot illustrated in Figure 6. [60,61].

In NCI plot we have observed that pics appear in weak interaction zone (Van der Waals interaction) for H_2 loaded systems, which indicates the non-covalent type interaction occure between model systems and H_2 molecules [25].

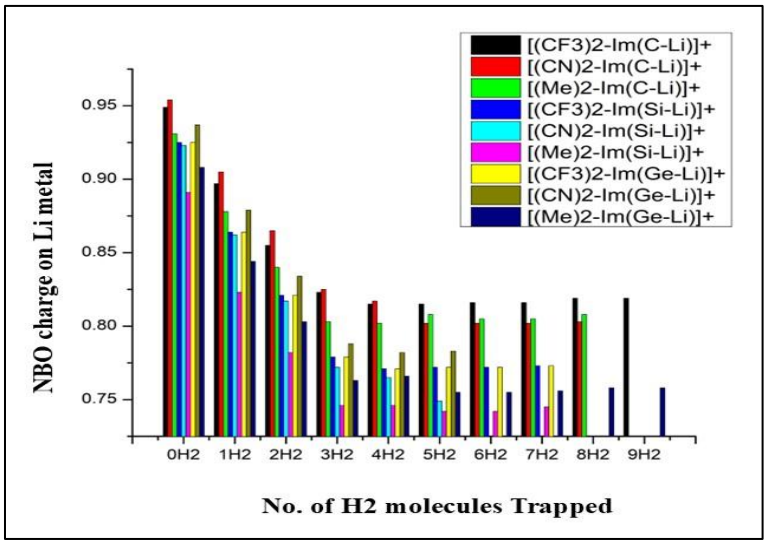

Figure 4: Variation of NBO charges on Li center in hosts and their sequential hydrogen trapped systems

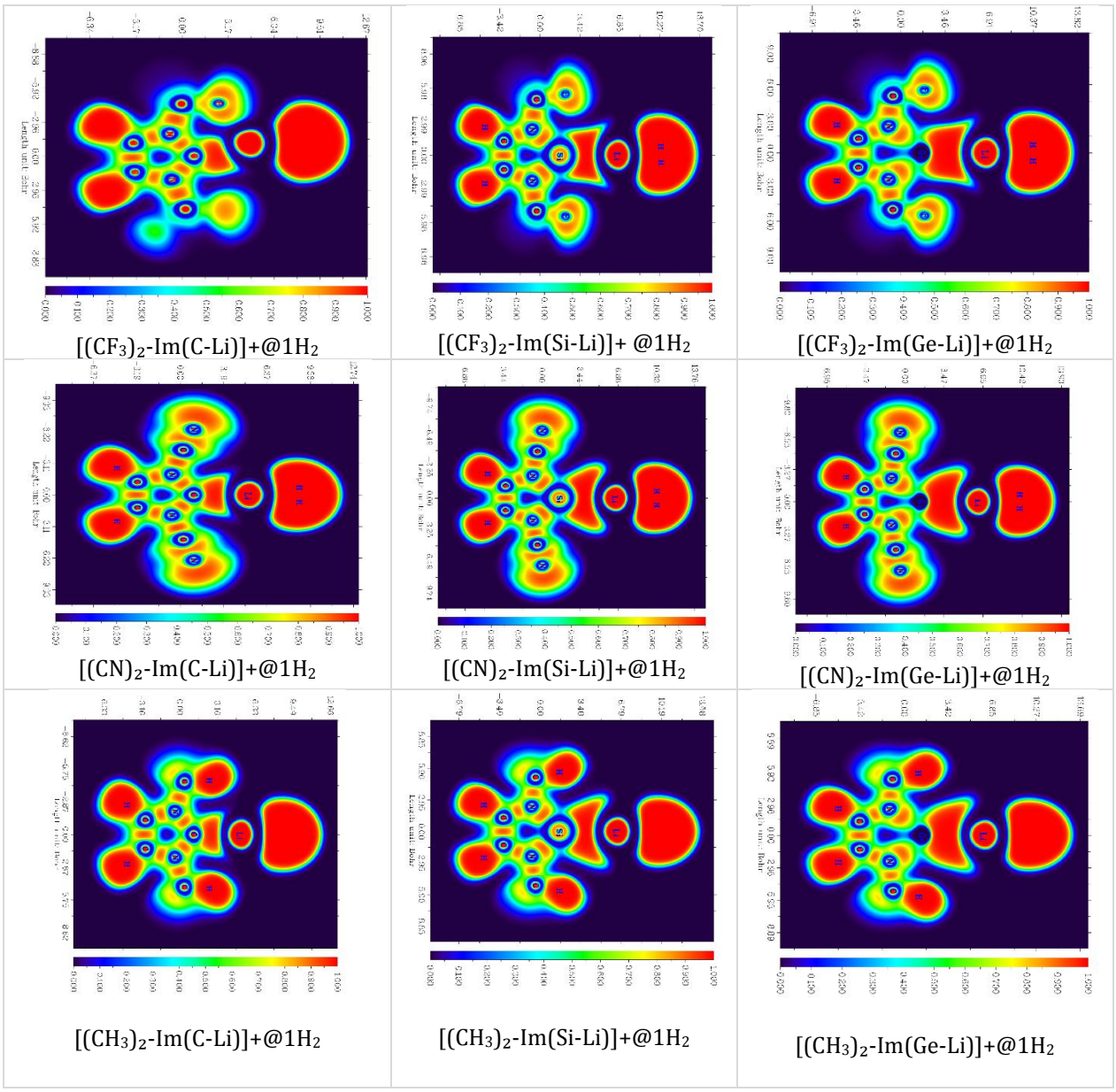

Figure 5: ELF plot of the electron density of the H_2 trapped different R substituted $[R_2\text{-Im(M-Li)}]^+@nH_2$ systems [where, R= -CF_3,-CN ,-CH_3, and M= C, Si, and Ge] at CAM-B3LYP/6–311+g (d, p) level of theory

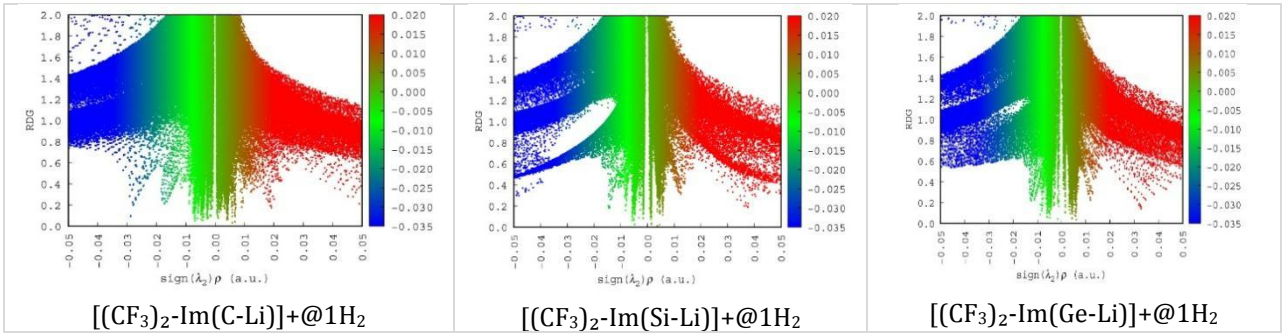

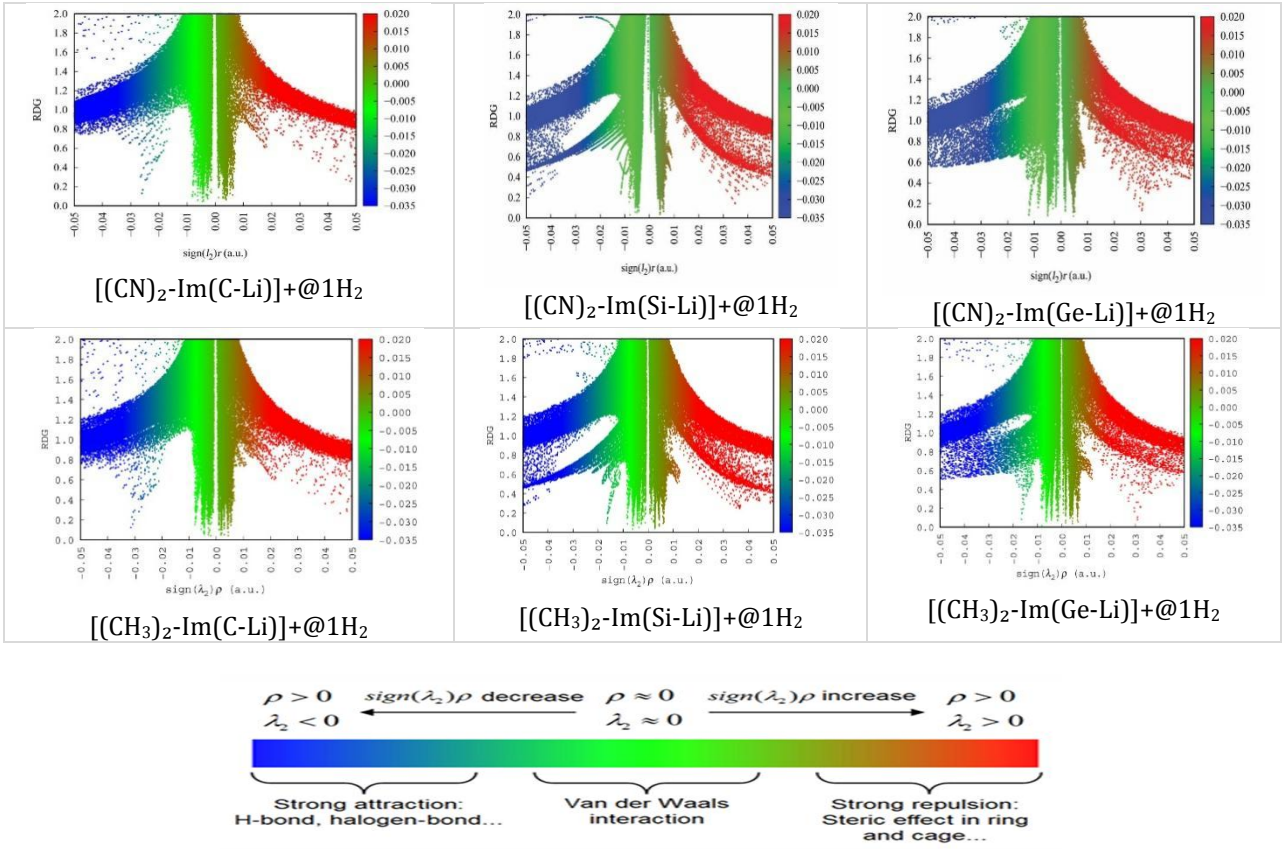

Figure 6: NCI plot of the H_2 trapped different R substituted $[R_2\text{-Im(M-Li)}]^+@nH_2$ systems [where R= $-CF_3$, -CN ,$-CH_3$, and M= C, Si, and Ge] at CAM-B3LYP/6–311+g (d, p) level of theory

Gibbs free energy indicate the trapping spontaneity of H_2 molecules of different systems at different temperature. The Gibbs free energy (ΔG) of different $[R_2\text{-Im(M-Li)}]+@nH_2$ systems, where, R = $-CF_3$, -CN, $-CH_3$, and M = C, Si, and Ge, varies with temperature, influencing their hydrogen trapping capabilities. At lower temperatures (200K), all systems exhibit negative ΔG values, indicating thermodynamically favorable hydrogen adsorption. The $[(CF_3)_2\text{-Im(C-Li)}]+@9H_2$ and $[(CH_3)_2\text{-Im(Ge-Li)}]+@9H_2$ systems show the lowest Gibbs free energy at -0.827 and -0.940, respectively, suggesting strong hydrogen binding. As the temperature rises to 250K, ΔG values increase, though some systems still retain negative values. By 298K, most systems shift toward positive ΔG, particularly for Ge- and Si-based complexes, implying reduced hydrogen adsorption favorability. The $[(CN)_2\text{-Im(C-Li)}]+@8H_2$ and $[(CF_3)_2\text{-Im(C-Li)}]_+@9H_2$ systems remain negative at this temperature, suggesting better retention. The trend highlights that lower temperatures favor hydrogen trapping, with Ge-based systems demonstrating the strongest binding at low temperatures. Maximum system shows spontaneity between 250K to 298K. But $[(CN)_2\text{-Im(C-Li)}]^+@8H_2$ and $[(CF3)_2\text{-Im(C-Li)}]^+@9H_2$ show spontaneity even at room temperature (Figure 7) [62,63].

Figure 5 indicates Gibbs free energy change at different temperature of highest H_2 trapped different R substituted $[R_2\text{-Im(M-Li)}]^+@nH_2$ systems [where, R= $-CF_3$, -CN ,$-CH_3$, and M= C, Si, and Ge] at CAM-B3LYP/6–311+g (d, p) level of theory.

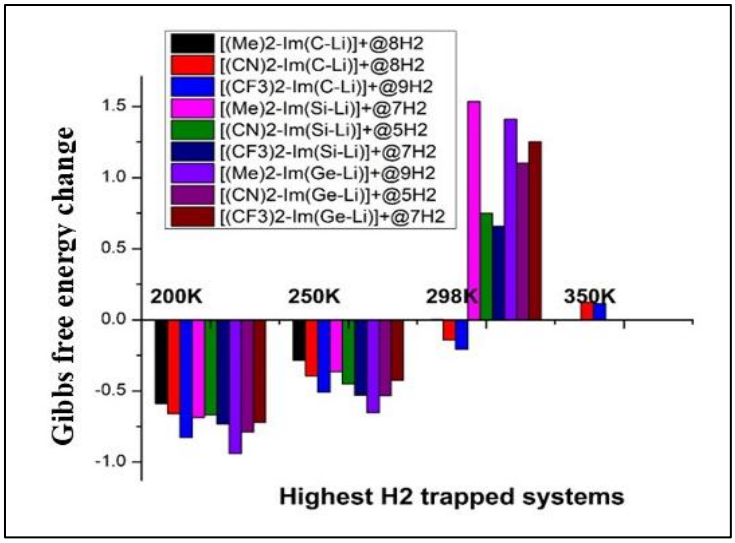

Figure 7: Gibbs free energy change at different temperature of highest H_2 trapped different R substituted [R_2-Im(M-Li)]$^+$@nH_2 systems [where, R= -CF_3, -CN ,-CH_3, and M= C, Si, and Ge] at CAM-B3LYP/6–311+g (d, p) level of theory

Gravimetric weight percent (wt%) of hydrogen in storage materials is the ratio of the mass of stored hydrogen to the total mass of the hydrogen storage system, expressed as a percentage. It indicates how efficiently a material can store hydrogen by weight. The gravimetric weight percentage (wt%) data for hydrogen storage presented in Table 3 highlights significant variation across different imidazole-based lithium-functionalized systems.

Notably, the Im(N-Li)+@5H_2 system exhibits a gravimetric wt% of 11.7%, positioning it as one of the high-performing candidates for hydrogen storage. However, when compared with [$(CH_3)_2$-Im(C-Li)]+@8H_2, which achieves an impressive 13.526%, Im(N-Li)+@5H_2 is slightly outperformed, suggesting that methyl substitution on the carbon-lithium framework offers superior hydrogen binding capacity. Analyzing global trends across the different systems, a clear pattern emerges: carbon-linked lithium complexes generally outperform their silicon and germanium counterparts in gravimetric hydrogen capacity. For example, [$(CH_3)_2$-Im(Si-Li)]+@7H_2 stores 10.595%, and [$(CH_3)_2$-Im(Ge-Li)]+@9H_2 stores 9.905%, both lower than the analogous carbon-lithium system. Furthermore, electron-withdrawing groups like CF_3 consistently correlate with lower wt% values (e.g., [$(CF_3)_2$-Im(Ge-Li)]+@7H_2 has only 4.915%), indicating that such groups may reduce hydrogen affinity, possibly due to their impact on electron density and steric hindrance. In summary, while Im(N-Li)+@5H_2 remains a strong candidate with competitive gravimetric efficiency, the [$(Me)_2$-Im(C-Li)]+@8H_2 system leads among the group, and the broader trend suggests that methyl-substituted, carbon-linked lithium imidazole frameworks offer the most promise for maximizing hydrogen storage [64,65].

To understand how each part of the complex contributes to its frontier orbitals, we carried out density of states (DOS) and partial density of states (PDOS) analyses on [(CH_3)2-Im(C-Li)]+@8H_2—the system with the highest gravimetric uptake. The resulting DOS/PDOS plots (Figure 8) show that both the HOMO and LUMO arise from a combination of contributions by the dimethyl-imidazolium core, the lithium ion, and the adsorbed hydrogen molecules.

Table 3: Gravimetric Wt% of highest H_2 trapped Im(N-Li)+@5H_2 and different R substituted [R_2-Im(M-Li)]$^+$@nH_2 systems [where R= -CF_3, -CN ,-CH_3, and M= C, Si, and Ge] at CAM-B3LYP/6–311+g (d, p) level of theory

Systems	Gravimetric Wt. %	Systems	Gravimetric Wt. %	Systems	Gravimetric Wt. %
Im(N-Li)+@5H_2	11.7	Im(N-Li)+@5H_2	11.7	Im(N-Li)+@5H_2	11.7
[(CF3)2-Im(C-Li)]+@9H_2	7.915	[(CN)2-Im(C-Li)]+@8H_2	11.422	[(CH_3)2-Im(C-Li)]+@8H_2	13.526
[(CF3)2-Im(Si-Li)]+@7H_2	5.851	[(CN)2-Im(Si-Li)]+@5H_2	6.669	[(CH_3)2-Im(Si-Li)]+@7H_2	10.595
[(CF3)2-Im(Ge-Li)]+@7H_2	4.915	[(CN)2-Im(Ge-Li)]+@5H_2	5.114	[(CH_3)2-Im(Ge-Li)]+@9H_2	9.905

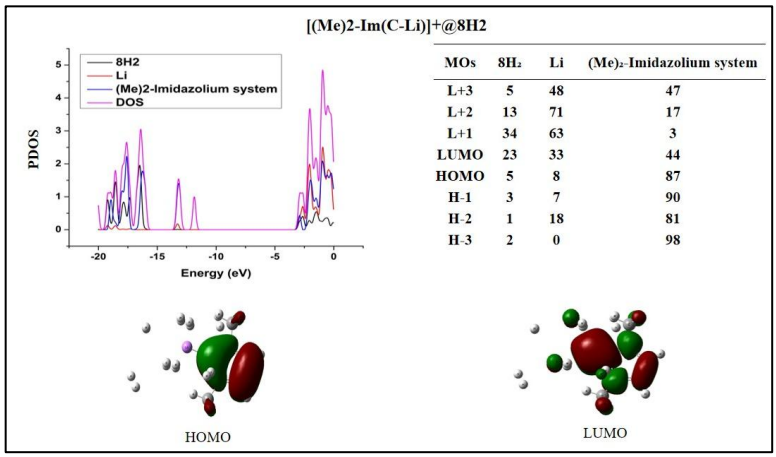

Figure 8: DOS and PDOS [Me_2-Im(C-Li)]+@8H_2 with % of contribution of $(Me)_2$-Imidazolium system, Li ion, and molecular hydrogen towards FMOs and their HOMO-LUMO picture at CAM-B3LYP/6–311+g (d, p) level of theory

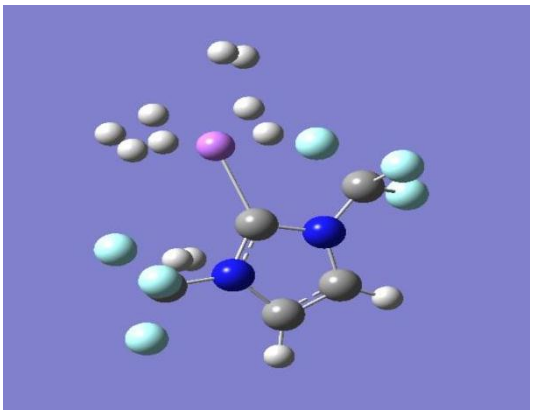

[a]

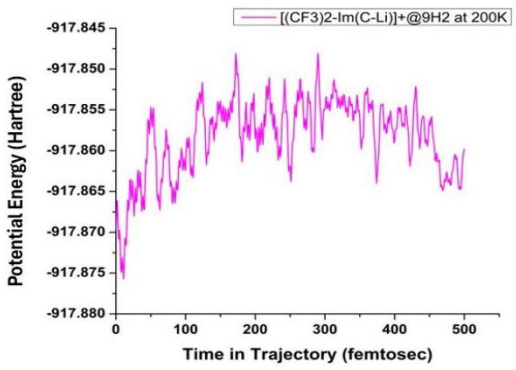

[b]

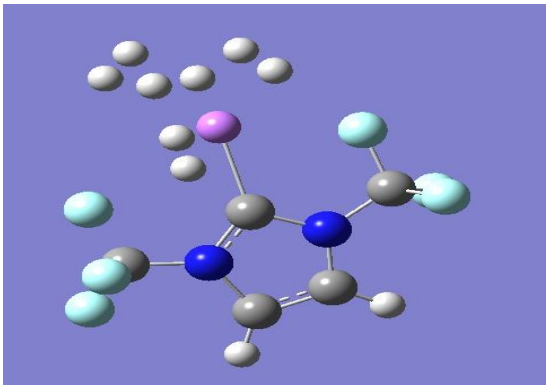

[c]

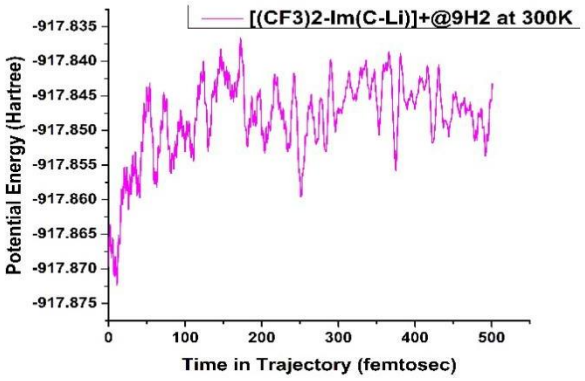
[(CF3)2-Im(C-Li)]+@9H2 at 300K
Potential Energy (Hartree)
-917.835
-917.840
-917.845
-917.850
-917.855
-917.860
-917.865
-917.870
-917.875
0
100
200
300
400
500
Time in Trajectory (femtosec)

[d]

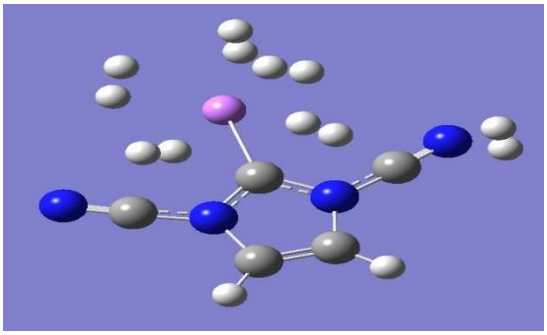

[e]

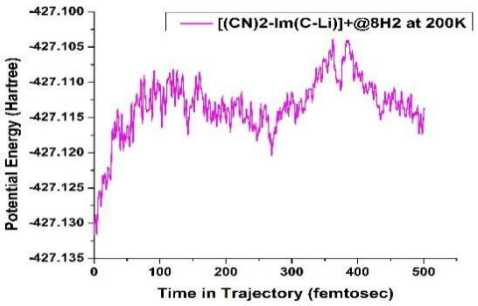
[(CN)2-Im(C-Li)]+@8H2 at 200K
Potential Energy (Hartree)
-427.100
-427.105
-427.110
-427.115
-427.120
-427.125
-427.130
-427.135
0
100
200
300
400
500
Time in Trajectory (femtosec)

[f]

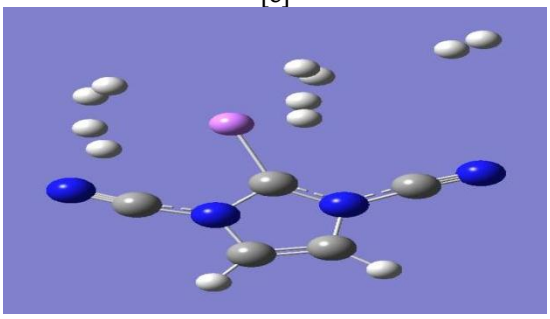

[g]

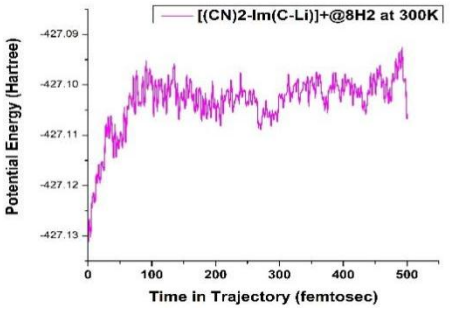
[(CN)2-Im(C-Li)]+@8H2 at 300K
Potential Energy (Hartree)
-427.09
-427.10
-427.11
-427.12
-427.13
0
100
200
300
400
500
Time in Trajectory (femtosec)

[h]

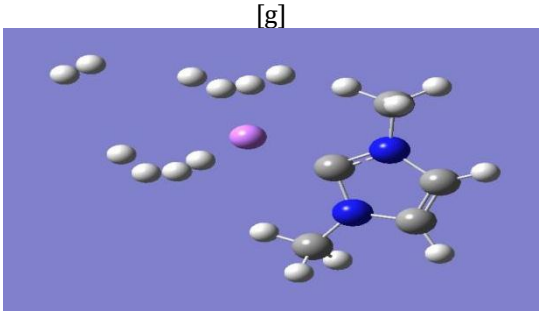

[i]

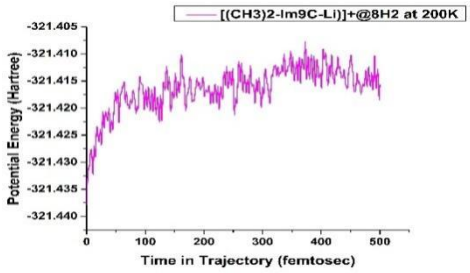
[(CH3)2-Im9C-Li)]+@8H2 at 200K
Potential Energy (Hartree)
-321.405
-321.410
-321.415
-321.420
-321.425
-321.430
-321.435
-321.440
0
100
200
300
400
500
Time in Trajectory (femtosec)

[j]

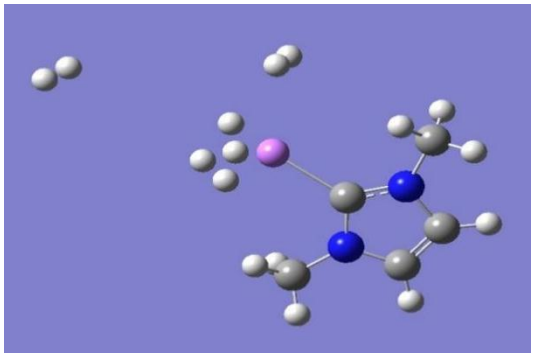

[k]

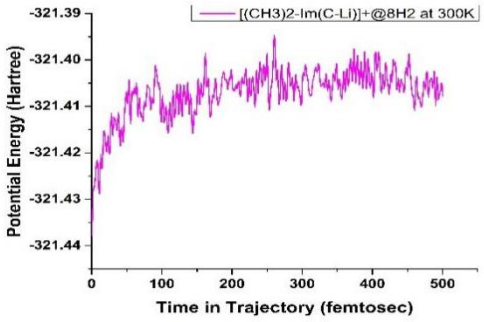

[l]

Figure 9: The simulated structures shown in (a), (c), (e), (g), (i), and (k) and the potential energy (E, A.U.) versus time (t, fs) of different R substituted [R_2-Im(M-Li)]+@nH_2 systems [where, R= -CF_3, -CN ,-CH_3 and M= C, Si, Ge] at CAM-B3LYP/6–311+g (d, p) level of theory at 200 K and 300 K, as well as at 500 fs, are shown in (b), (d), (f), (h), (j), and (l)

Atom-centered density matrix propagation (ADMP) simulations have been performed to investigate the kinetic stability of various R-substituted [R_2-Im(M-Li)]+@nH_2 complexes, where R represents -CF_3, -CN, or -CH_3, and M stands for C, Si, or Ge. The simulations were conducted at two different temperatures (200 K and 300 K). A 1 fs time step and a velocity scaling thermostat were employed to maintain a constant temperature throughout the simulations. The potential energy (Hartree) versus time (femtosec) graphs is presented in Figure 9. Based on Figure 9, it is evident that the complexes can retain H_2 molecules at lower temperatures for up to 500 fs. However, desorption begins as the temperature rises. At ambient temperature, some molecular H_2 remains attached to the systems. This suggests that the Li metal-decorated model systems can maintain stability and adsorb H_2 even at room temperature [66,67].

Conclusion

The present study demonstrates that the hydrogen storage potential of R_2 substituted [R_2-Im(M-Li)]+@nH_2 systems is strongly influenced by both the choice of substituent (–CF_3, –CN, –CH_3) and the central metal atom (C, Si, and Ge). Carbon-based complexes exhibit superior gravimetric storage capacities and more favorable adsorption energies, with –CN and –CH_3 substitutions promoting stronger electron-accepting behavior and enhanced hydrogen binding. The adsorption process is primarily governed by non-covalent interactions, as confirmed by ELF and NCI analyses, and is further supported by NBO charge redistribution on Li metal center upon H_2 uptake. Moreover, At 200-250 K, all complexes bind H_2 spontaneously, but by 298 K only the carbon-based systems remain favorable—silicon and germanium analogues no longer do. The global focus is shifting towards hydrogen (H_2) as a green fuel, with several countries already adopting it as part of their Mission. As a result, the search for suitable hydrogen storage materials has become a topic of high relevance. Previous studies have reported promising hydrogen storage materials, where theoretical predictions align well with experimental results [68,69]. In the present study, all systems investigated show thermodynamically feasible adsorption at room temperature and near room temperature, though further investigation through synthetic approaches is required. The materials we selected are commonly available chemicals, and we anticipate that in the near future, they will be synthesized. Our theoretical insights are expected to guide experimental researchers in understanding the stoichiometry and thermochemical behavior of these systems. Overall, these findings provide a compelling basis for the design of efficient hydrogen storage materials, highlighting the critical role

of molecular tuning in optimizing performance for sustainable energy applications.

Acknowledgements

GR acknowledge the financial support from SERB project (TAR/2022/000162), Govt. of India. The article is dedicated to Smt. Gayatri Roymahapatra, (mother of GR) in her 67th Birthday.

Orcid

Abhishek Bag: 0009-0001-8390-9847
Anupam Aash: 0009-0001-0880-2310
Dilip K. Debnath: 0000-0001-7158-0813
G. Naaresh Reddy: 0000-0002-5014-9036
Gourisankar Roymahapatra: 0000-0002-8018-5206

Reference

[1]. L. Schlapbach, A. Züttel, Hydrogen-storage materials for mobile applications, *Nature*, **2001**, *414*, 353-358. [Crossref], [Google Scholar], [Publisher]
[2]. Y. Zhang, Z. Jia, Z. Yuan, T. Yang, Y. Qi, D. Zhao, Development and application of hydrogen storage, *Journal of Iron and Steel Research International*, **2015**, *22*, 757-770. [Crossref], [Google Scholar], [Publisher]
[3]. J. Yang, A. Sudik, C. Wolverton, D.J. Siegel, High capacity hydrogen storage materials: attributes for automotive applications and techniques for materials discovery, *Chemical Society Reviews*, **2010**, *39*, 656-675. [Crossref], [Google Scholar], [Publisher]
[4]. X. Xu, Y. Dong, Q. Hu, N. Si, C. Zhang, Electrochemical hydrogen storage materials: state-of-the-art and future perspectives, *Energy & Fuels*, **2024**, *38*, 7579-7613. [Crossref], [Google Scholar], [Publisher]
[5]. T.K. Mandal, D.H. Gregory, Hydrogen storage materials: present scenarios and future directions, *Annual Reports Section" A"(Inorganic Chemistry)*, **2009**, *105*, 21-54. [Crossref], [Google Scholar], [Publisher]
[6]. P. Jena, Materials for hydrogen storage: past, present, and future, *The Journal of Physical Chemistry Letters*, **2011**, *2*, 206-211. [Crossref], [Google Scholar], [Publisher]
[7]. S.K. Dewangan, M. Mohan, V. Kumar, A. Sharma, B. Ahn, A comprehensive review of the prospects for future hydrogen storage in materials-application and outstanding issues, *International Journal of Energy Research*, **2022**, *46*, 16150-16177. [Crossref], [Google Scholar], [Publisher]
[8]. P. Preuster, A. Alekseev, P. Wasserscheid, Hydrogen storage technologies for future energy systems, *Annual review of chemical and biomolecular engineering*, **2017**, *8*, 445-471. [Crossref], [Google Scholar], [Publisher]
[9]. A. Züttel, Materials for hydrogen storage, *Materials today*, **2003**, *6*, 24-33. [Crossref], [Google Scholar], [Publisher]
[10]. G. Roymahapatra, M.K. Dash, S. Sinha, G. Ch, Z. Guo, Theoretical investigation of hydrogen adsorption efficiency of [Oxadiazole-xLi+] complexes (x= 1, 2): in pursuit of green fuel storage, *Engineered Science*, **2022**, *19*, 114-124. [Crossref], [Google Scholar]
[11]. M.K. Dash, S. Sinha, H.S. Das, G.C. De, S. Giri, G. Roymahapatra, H2 storage capacity of Li-doped five member aromatic heterocyclic superalkali complexes; an in silico study, *Sustainable Energy Technologies and Assessments*, **2022**, *52*, 102235. [Crossref], [Google Scholar], [Publisher]
[12]. M.K. Dash, S. Das, S. Giri, G.C. De, G. Roymahapatra, Comprehensive in silico study on lithiated Triazine isomers and its H2 storage efficiency, *Journal of the Indian Chemical Society*, **2021**, *98*, 100134. [Crossref], [Google Scholar], [Publisher]
[13]. R. Parida, M.K. Dash, S. Giri, G. Roymahapatra, Aromatic N-Heterocyclic superalkali M@ C4H4N2 complexes (M= Li, Na, K); A promising potential hydrogen storage system, *Journal of the Indian Chemical Society*, **2021**, *98*, 100065. [Crossref], [Google Scholar], [Publisher]
[14]. R.K. Sahoo, S. Sahu, Reversible hydrogen storage capacity of Li and Sc doped novel C8N8 cage: Insights from density functional theory, *International Journal of Energy Research*, **2022**, *46*, 22585-22600. [Crossref], [Google Scholar], [Publisher]
[15]. S. Chattaraj, K. Srinivasu, S. Mondal, S.K. Ghosh, Hydrogen trapping ability of the pyridine–lithium+ (1: 1) complex, *The Journal of*

Physical Chemistry A, **2015**, *119*, 3056-3063. [Crossref], [Google Scholar], [Publisher]
[16]. M.K. Dash, S.D. Chowdhury, R. Chatterjee, S. Maity, G. Roymahapatra, M. Huang, M. Nath, Z. Guo, Computational investigation on lithium fluoride for efficient hydrogen storage system, *Engineered Science*, **2022**, *18*, 98-104. [Crossref], [Google Scholar],
[17]. G. Roymahapatra, M.K. Dash, A. Ghosh, A. Bag, S. Mishra, S. Maity, Hydrogen storage on lithium chloride/lithium bromide surface at cryogenic temperature, *ES Energy & Environment*, **2022**, *18*, 90-100. [Crossref], [Google Scholar]
[18]. S. Pan, S. Giri, P.K. Chattaraj, A computational study on the hydrogen adsorption capacity of various lithium—Doped boron hydrides, *Journal of Computational Chemistry*, **2012**, *33*, 425-434. [Crossref], [Google Scholar], [Publisher]
[19]. Q. Sun, P. Jena, Q. Wang, M. Marquez, First-principles study of hydrogen storage on Li12C60, *Journal of the American Chemical Society*, **2006**, *128*, 9741-9745. [Crossref], [Google Scholar], [Publisher]
[20]. A. Blomqvist, C.M. Araújo, P. Srepusharawoot, R. Ahuja, Li-decorated metal–organic framework 5: A route to achieving a suitable hydrogen storage medium, *Proceedings of the National Academy of Sciences*, **2007**, *104*, 20173-20176. [Crossref], [Google Scholar], [Publisher]
[21]. R.Y. Sathe, T.D. Kumar, Reversible hydrogen adsorption in Li functionalized [1, 1] paracyclophane, *International Journal of Hydrogen Energy*, **2020**, *45*, 12940-12948. [Crossref], [Google Scholar], [Publisher]
[22]. A. Bag, M.K. Dash, S. Giri, G.C. De, G. Roymahapatra, CRC Press/Taylor & Francis Group, 2023. ISBN 9781032528540, [Crossref], [Google Scholar], [Publisher]
[23]. A. Bag, S. Giri, P. Dhaiveegan, R.T. Jalgham, G. Ch, J. Ganguly, G. Roymahapatra, A theoretical study on Au (I) decorated isomeric triazine complexes as a new class of hydrogen storage materials, *ES Energy & Environment*, **2024**, *23*, 1115. [Crossref], [Google Scholar]
[24]. A. Bag, S. Sinha, H.S. Das, S. Giri, G. Ch, S. Maity, B.B. Xu, Z. Guo, J. Ganguly, G. Roymahapatra, Hydrogen storage efficiency of the Ag (I)/Au (I) decorated five-member aromatic heterocyclic (AH) compounds: A theoretical investigation, *Engineered Science*, **2023**, *28*, 1062. [Crossref], [Google Scholar]
[25]. A. Bag, G.C. De, S. Bhattacharyya, B. Bepari, H.S. Das, S. Bandaru, G. Roymahapatra, Ag (I) decorated isomeric Triazine complexes as efficient Hydrogen storage materials-A theoretical investigation, *Chemistry of Inorganic Materials*, **2025**, 100093. [Crossref], [Google Scholar], [Publisher]
[26]. C. Tarhan, M.A. Çil, A study on hydrogen, the clean energy of the future: Hydrogen storage methods, *Journal of Energy Storage*, **2021**, *40*, 102676. [Crossref], [Google Scholar], [Publisher]
[27]. M. Rasul, M. Hazrat, M. Sattar, M. Jahirul, M. Shearer, The future of hydrogen: Challenges on production, storage and applications, *Energy Conversion and Management*, **2022**, *272*, 116326. [Crossref], [Google Scholar], [Publisher]
[28]. J. Ren, N.M. Musyoka, H.W. Langmi, M. Mathe, S. Liao, Current research trends and perspectives on materials-based hydrogen storage solutions: A critical review, *International journal of hydrogen energy*, **2017**, *42*, 289-311. [Crossref], [Google Scholar], [Publisher]
[29]. A. Dillon, M. Heben, Hydrogen storage using carbon adsorbents: past, present and future, *Applied Physics A*, **2001**, *72*, 133-142. [Crossref], [Google Scholar], [Publisher]
[30]. E. David, An overview of advanced materials for hydrogen storage, *Journal of materials processing technology*, **2005**, *162*, 169-177. [Crossref], [Google Scholar], [Publisher]
[31]. N. Musheer, M. Yusuf, A. Choudhary, M. Shahid, Recent advances in heavy metal remediation using biomass-derived carbon materials, *Advanced Journal of Chemistry - Section B,* **2024**, 6(3), 284-345. [Crossref], [Google Scholar], [Publisher]
[32]. R.G. Parr, R.G. Pearson, Absolute hardness: companion parameter to absolute electronegativity, *Journal of the American Chemical Society*, **1983**, *105*, 7512-7516. [Crossref], [Google Scholar], [Publisher]
[33].D.M. Zaini, D. Syafi'ah, R. Rini, T. Anugrahini, U. Ahmad, A. Rahmi, Z.F. Arief, Foundational study on the stability limitations

of catechin from Uncaria gambir in aqueous systems: Basis for industrial applications, Asian Journal of Green Chemistry, **2025**, 9(3), 573–586. [Crossref], [Publisher]
[34]. S. Sengupta, P. Chattaraj, The quantum theory of motion and signatures of chaos in the quantum behaviour of a classically chaotic system, *Physics Letters A*, **1996**, *215*, 119-127. [Crossref], [Google Scholar], [Publisher]
[35]. P. Chattara, Electronegativity and hardness: A density functional treatment, *Journal of the Indian Chemical Society*, **1992**, *69*, 173-183. [Crossref], [Google Scholar], [Publisher]
[36]. R.G. Parr, R.A. Donnelly, M. Levy, W.E. Palke, Electronegativity: The density functional viewpoint, *The Journal of Chemical Physics*, **1978**, *68*, 3801-3807. [Crossref], [Google Scholar], [Publisher]
[37]. R.G. Parr, L.v. Szentpály, S. Liu, Electrophilicity index, *Journal of the American Chemical Society*, **1999**, *121*, 1922-1924. [Crossref], [Google Scholar], [Publisher]
[38]. P.K. Chattaraj, U. Sarkar, D. Roy, Electronic structure principles and aromaticity, *Journal of Chemical Education*, **2007**, *84*, 354. [Crossref], [Google Scholar], [Publisher]
[39]. P.K. Chattaraj, D.R. Roy, Update 1 of: electrophilicity index, *Chemical Reviews*, **2007**, *107*, PR46-PR74. [Crossref], [Google Scholar], [Publisher]
[40]. R.G. Parr, Density functional theory of atoms and molecules, *Horizons of Quantum Chemistry: Proceedings of the Third International Congress of Quantum Chemistry Held at Kyoto, Japan*, **1979**, 5-15. [Crossref], [Google Scholar], [Publisher]
[41]. R.G. Parr, R.G. Pearson, Absolute hardness: Companion parameter to absolute electronegativity, *Journal of the American Chemical Society*, **1983**, *105*, 7512-7516. [Crossref], [Google Scholar], [Publisher]
[42]. N. Mardirossian, M. Head-Gordon, Thirty years of density functional theory in computational chemistry: An overview and extensive assessment of 200 density functionals, *Molecular Physics*, **2017**, *115*, 2315-2372. [Crossref], [Google Scholar], [Publisher]
[43]. P. Makkar, N.N. Ghosh, A review on the use of DFT for the prediction of the properties of nanomaterials, *RSC advances*, **2021**, *11*, 27897-27924. [Crossref], [Google Scholar], [Publisher]
[44]. D. Chakraborty, P.K. Chattaraj, Conceptual density functional theory based electronic structure principles, *Chemical Science*, **2021**, *12*, 6264-6279. [Crossref], [Google Scholar], [Publisher]
[45]. P. Geerlings, E. Chamorro, P.K. Chattaraj, F. De Proft, J.L. Gázquez, S. Liu, C. Morell, A. Toro-Labbé, A. Vela, P. Ayers, Conceptual density functional theory: Status, prospects, issues, *Theoretical Chemistry Accounts*, **2020**, *139*, 36. [Crossref], [Google Scholar], [Publisher]
[46]. P.K. Chattaraj, Chemical reactivity theory: A density functional view, *CRC Press*, **2009**. [Crossref], [Google Scholar], [Publisher]
[47]. A. Stanger, NICS–past and present, *European Journal of Organic Chemistry*, **2020**, *2020*, 3120-3127. [Crossref], [Google Scholar], [Publisher]
[48]. Z. Chen, C.S. Wannere, C. Corminboeuf, R. Puchta, P.v.R. Schleyer, Nucleus-independent chemical shifts (NICS) as an aromaticity criterion, *Chemical reviews*, **2005**, *105*, 3842-3888. [Crossref], [Google Scholar], [Publisher]
[49]. R. Parida, M. Rath, S. Sinha, G. Roymahapatra, S. Giri, Organic and inorganic benzene transform to superalkalis: An in silico study, *Journal of Indian Chemical Society*, **2020**, *97*, 2689-2697. [Crossref], [Google Scholar], [Publisher]
[50]. S. Sinha, S. Das, G. Roymahapatra, S. Giri, Stability, reactivity, and aromaticity of benzene, borazine, and hexasilabenzene, *International Journal of HIT Transaction on ECCN*, **2020**, *6*, 7-13. [Crossref], [Google Scholar]
[51]. R. Parida, S. Das, L.J. Karas, J.I.-C. Wu, G. Roymahapatra, S. Giri, Superalkali ligands as a building block for aromatic trinuclear Cu (i)–NHC complexes, *Inorganic Chemistry Frontiers*, **2019**, *6*, 3336-3344. [Crossref], [Google Scholar], [Publisher]
[52]. T. Lu, F. Chen, Multiwfn: A multifunctional wavefunction analyzer, *Journal of Computational Chemistry*, **2012**, *33*, 580-592. [Crossref], [Google Scholar], [Publisher]
[53]. A. Ebrahimi, M. Izadyar, M. Khavani, Theoretical design of a new hydrogen storage based on the decorated phosphorene nanosheet by alkali metals, *Journal of Physics and*

Chemistry of Solids, **2023**, *178*, 111354. [Crossref], [Google Scholar], [Publisher]
[54]. A. Johnson, Energy crisis and the path to salvation: Hydrogen, the driving force of a clean future, *Journal of Engineering in Industrial Research*, **2025**. [Crossref], [Publisher]
[55]. S. Mondal, Structure, bonding, and interaction with molecular hydrogen of the β-D-glucopyranose—silver+ (1: 1) complex, *Journal of Physical Organic Chemistry*, **2023**, *36*, e4448. [Crossref], [Google Scholar], [Publisher]
[56]. A. Züttel, Hydrogen storage methods, *Naturwissenschaften*, **2004**, *91*, 157-172. [Crossref], [Google Scholar], [Publisher]
[57]. Z. Ao, F. Peeters, High-capacity hydrogen storage in Al-adsorbed graphene, *Physical Review B—Condensed Matter and Materials Physics*, **2010**, *81*, 205406. [Crossref], [Google Scholar], [Publisher]
[58]. C.G. Zhang, R. Zhang, Z.X. Wang, Z. Zhou, S.B. Zhang, Z. Chen, Ti-Substituted Boranes as Hydrogen Storage Materials: A Computational Quest for the Ideal Combination of Stable Electronic Structure and Optimal Hydrogen Uptake, *Chemistry–A European Journal*, **2009**, *15*, 5910-5919. [Crossref], [Google Scholar], [Publisher]
[59]. M.Y. Mehboob, R. Hussain, F. Younas, S. Jamil, M.M.A. Iqbal, K. Ayub, N. Sultana, M.R.S.A. Janjua, Computation assisted design and prediction of alkali-metal-centered B12N12 nanoclusters for efficient H2 adsorption: new hydrogen storage materials, *Journal of Cluster Science*, **2023**, *34*, 1237-1247. [Crossref], [Google Scholar], [Publisher]
[60]. H.O. Edet, H. Louis, I. Benjamin, M. Gideon, T.O. Unimuke, S.A. Adalikwu, A.D. Nwagu, A.S. Adeyinka, Hydrogen storage capacity of C12X12 (X= N, P, and Si), *Chemical Physics Impact*, **2022**, *5*, 100107. [Crossref], [Google Scholar], [Publisher]
[61]. E.S. Osipova, E.A. Gladkov, Heracleum sosnowskyi Manden, as a source of valuable chemicals (elimination with utility), *Chemical Methodologies*, **2024**, 8(12), 944-956. [Crossref], [Google Scholar], [Publisher]
[62]. C. Wolverton, D.J. Siegel, A. Akbarzadeh, V. Ozoliņš, Discovery of novel hydrogen storage materials: an atomic scale computationalapproach, *Journal of Physics: Condensed Matter*, **2008**, *20*, 064228. [Crossref], [Google Scholar], [Publisher]
[63]. S. Niaz, T. Manzoor, A.H. Pandith, Hydrogen storage: Materials, methods and perspectives, *Renewable and Sustainable Energy Reviews*, **2015**, *50*, 457-469. [Crossref], [Google Scholar], [Publisher]
[64]. U.B. Demirci, P. Miele, Chemical hydrogen storage: 'material'gravimetric capacity versus 'system'gravimetric capacity, *Energy & Environmental Science*, **2011**, *4*, 3334-3341. [Crossref], [Google Scholar], [Publisher]
[65]. E. Masika, R. Mokaya, Exceptional gravimetric and volumetric hydrogen storage for densified zeolite templated carbons with high mechanical stability, *Energy & Environmental Science*, **2014**, *7*, 427-434. [Crossref], [Google Scholar], [Publisher]
[66.] V. Kalamse, N. Wadnerkar, A. Deshmukh, A. Chaudhari, C2H2M (M= Ti, Li) complex: A possible hydrogen storage material, *International Journal of Hydrogen Energy*, **2012**, *37*, 3727-3732. [Crossref], [Google Scholar], [Publisher]
[67]. R.Y. Sathe, S. Kumar, T.J.D. Kumar, First-principles study of hydrogen storage in metal functionalized [4, 4] paracyclophane, *International Journal of Hydrogen Energy*, **2018**, *43*, 5680-5689. [Crossref], [Google Scholar], [Publisher]
[68]. J. Lyu, R.R. Elman, L.A. Svyatkin, V.N. Kudiiarov, Theoretical and experimental research of hydrogen solid solution in Mg and Mg-Al system, *Materials*, **2022**, *15*, 1667. [Crossref], [Google Scholar], [Publisher]
[69]. H. Nishihara, S. Ittisanronnachai, H. Itoi, L.-X. Li, K. Suzuki, U. Nagashima, H. Ogawa, T. Kyotani, M. Ito, Experimental and theoretical studies of hydrogen/deuterium spillover on Pt-loaded zeolite-templated carbon, *The Journal of Physical Chemistry C*, **2014**, *118*, 9551-9559. [Crossref], [Google Scholar], [Publisher]